Unsteady Propagation and Mean Corrections in Open-Jet and Kevlar Wind Tunnels

Christopher J. Bahr* and Florence V. Hutcheson†
NASA Langley Research Center, Hampton, Virginia, 23681

Daniel J. Stead‡
Science and Technology Corporation, Hampton, Virginia, 23666

Two types of aeroacoustic wind tunnel test section configurations have been tested in the NASA Langley Quiet Flow Facility. The first is a more traditional open-jet configuration, where test section flow passes unbounded through the facility anechoic chamber. The second is a Kevlar panel configuration, where a tensioned Kevlar sheet constrains the test section flow from the facility anechoic chamber. For both configurations, acoustic instrumentation is in the surrounding quiescent space. Both configurations are evaluated with a laser-based pulsed acoustic source, which provides unique capability for assessing the facility unsteady acoustic propagation characteristics. Metrics based on the wander and spread of the pulses are evaluated and show that measurements using Kevlar walls experience dramatically reduced unsteady effects when compared to the open-jet configuration. This leads to a corresponding improvement in coherence between microphones with the Kevlar configuration, by reducing the variation in magnitude and phase differences between channels. Magnitude corrections for propagation through Kevlar as compared to open-jet propagation are calculated. While limitations in the experimental setup make quantitative analysis difficult, qualitative analysis shows Kevlar magnitude corrections similar to those determined in previous literature. Directivity effects beyond those already present for open-jet configurations are minimal. The background noise produced by the Kevlar is found to be its one drawback when compared with the open-jet configuration, showing significantly greater levels at high frequencies.

I. Nomenclature

C	=	block-by-block normalized cross-spectral term
CV	=	coefficient of variation

*Senior Research Engineer, Aeroacoustics Branch, Mail Stop 461, AIAA Associate Fellow, christopher.j.bahr@nasa.gov (Corresponding author)
†Senior Research Engineer, Aeroacoustics Branch, Mail Stop 461, AIAA Associate Fellow
‡Senior Engineer, Mail Stop 461

Presented as Paper 2018-3118 at the 24th AIAA/CEAS Aeroacoustics Conference, Atlanta, GA, 25–29 June 2018.

E = block-to-block ensemble average operation

H = propagation transfer function

i, j = microphone indices

Kev = measurement in Kevlar test configuration

$Open$ = measurement in open-jet test configuration

rm = reference microphone

T_{rel} = relative transmission coefficient between Kevlar and open-jet configurations

t_a = acoustic pulse arrival time

X = source signal

Y = microphone measurement

Y_0 = measurement shifted in time by t_a for a given block

$Y_{0,m}$ = measurement shifted in time by the mean of t_a across all blocks in a record

γ = coherence

II. Introduction

Aeroacoustic wind tunnels are often configured such that acoustic instrumentation is separated from the facility's test section flow, minimizing measurement contamination by hydrodynamic pressure fluctuations. One facility concept that accomplishes this is the open-jet test section, where instrumentation is separated from the test section flow by a free shear layer [1]. Another facility concept is the Kevlar-walled test section. Here, a sheet of Kevlar constrains the test section flow while allowing acoustic waves to pass through [2, 3]. In both facility types, the acoustic signal of interest must traverse an interface, which bounds the test section flow from the quiescent surrounding medium. This boundary influences the propagation of the acoustic waves as they pass through it. In the mean sense, the interface between two media refracts the acoustic waves, leading to a deterministic change in both the direction of wave propagation and the level of the signal [4, 5]. In the unsteady sense, the acoustic signal passes through either a turbulent free shear layer or a turbulent boundary layer on the Kevlar surface. Both classes of turbulent shear flow scatter the acoustic waves of interest, leading to a stochastic change in both the direction of propagation and the level of the signal [6].

The stochastic scattering of the acoustic waves manifests itself in several ways, depending on how the acoustic data of interest are evaluated. In the frequency domain, the scattering can appear as coherence loss, where the magnitude and phase of coherent signals are randomized. This randomization leads to a reduction in average cross-spectral magnitude and, thus, the coherence. It can appear as a level reduction for a single microphone when multiple, partially-coherent sources are being measured [7], or as a degradation of the cross-spectra between pairs of microphones for single-source or incoherent field measurements [8–10]. For tonal acoustic signals, scattering broadens the otherwise sharp spectral shape [11, 12]. In microphone phased array processing, this degradation can lead to a blurring effect in the source maps, demonstrated, for example, in recent airframe noise testing [13, 14]. In the time domain, this scattering can be observed with acoustic pulses as *spread* and *wander*, where spread is defined as a change in pulse form or shape, and wander is defined as a change in pulse propagation time. Wander is considered the dominant mechanism in "weak scattering" assumptions [15, 16], and may be correctable with in situ techniques [17].

Recently, a cross-facility test campaign utilized a pulsed acoustic source to characterize the influence of flow effects on noise shielding by a canonical airfoil [18–20]. The extensive use of a laser-based plasma source provided an opportunity to study acoustic propagation of pulses through a turbulent shear flow. In the NASA Langley Quiet Flow Facility, microphones were located out of the facility test section to measure the pulsed signal. This was done both for the facility's baseline open-jet configuration, as well as with a Kevlar panel bounding the test section flow on one side. The setup allowed for the direct comparison of the relative influence of both test section interface types on acoustic pulse propagation. This paper proceeds with a discussion of the test setup and data processing, followed by an assessment of the unsteady propagation behavior of pulses through the two interface types. The magnitude corrections for the Kevlar panel are calculated, prior to a brief discussion on the measured pulse spectra. Finally, the background noise characteristics of both test section boundaries are shown.

III. Test Setup and Data Processing

A. Test configuration

The details of the test setup for the overall measurement campaign are documented elsewhere [20]. To briefly summarize, an Nd:YAG (here a Gemini PIV 120 mJ, 532 nm, 3-5 ns pulse width) laser is focused to a point in space using a set of 7.62 cm diameter achromatic expansion, collimating, and focusing lenses, generating a plasma-induced shock wave [21]. This shock propagates and decays to a linear acoustic wave, acting as a minimally-intrusive acoustic point source [22]. Such a source is particularly appealing for aeroacoustic wind tunnel testing, as most sources placed in a facility test section will alter the test section flow field and generate undesirable aerodynamic noise. In addition to the current noise shielding measurement campaign, this source type has been used in open-jet wind tunnels to evaluate mean refraction effects and mean beamforming corrections [23, 24].

The data used in this study were acquired in the NASA Langley Quiet Flow Facility (QFF). QFF is an anechoic open-jet wind tunnel facility equipped with a 2- by 3-foot rectangular nozzle. For the unsteady propagation portion of this study, the NACA 0012 and inflow microphone from the shielding test were removed. Sketches of the experimental setup are shown in Fig. 1. The Kevlar panel consisted of a custom woven sheet of Kevlar 49 Style 120, which nominally has 34 fibers per inch and is 0.003 inches thick [25]. This sheet was tensioned to approximately 100 lbf/ft (1500 N/m). Outside of the test section flow, an arc of 1/8" microphones with conventional grid caps was installed. In

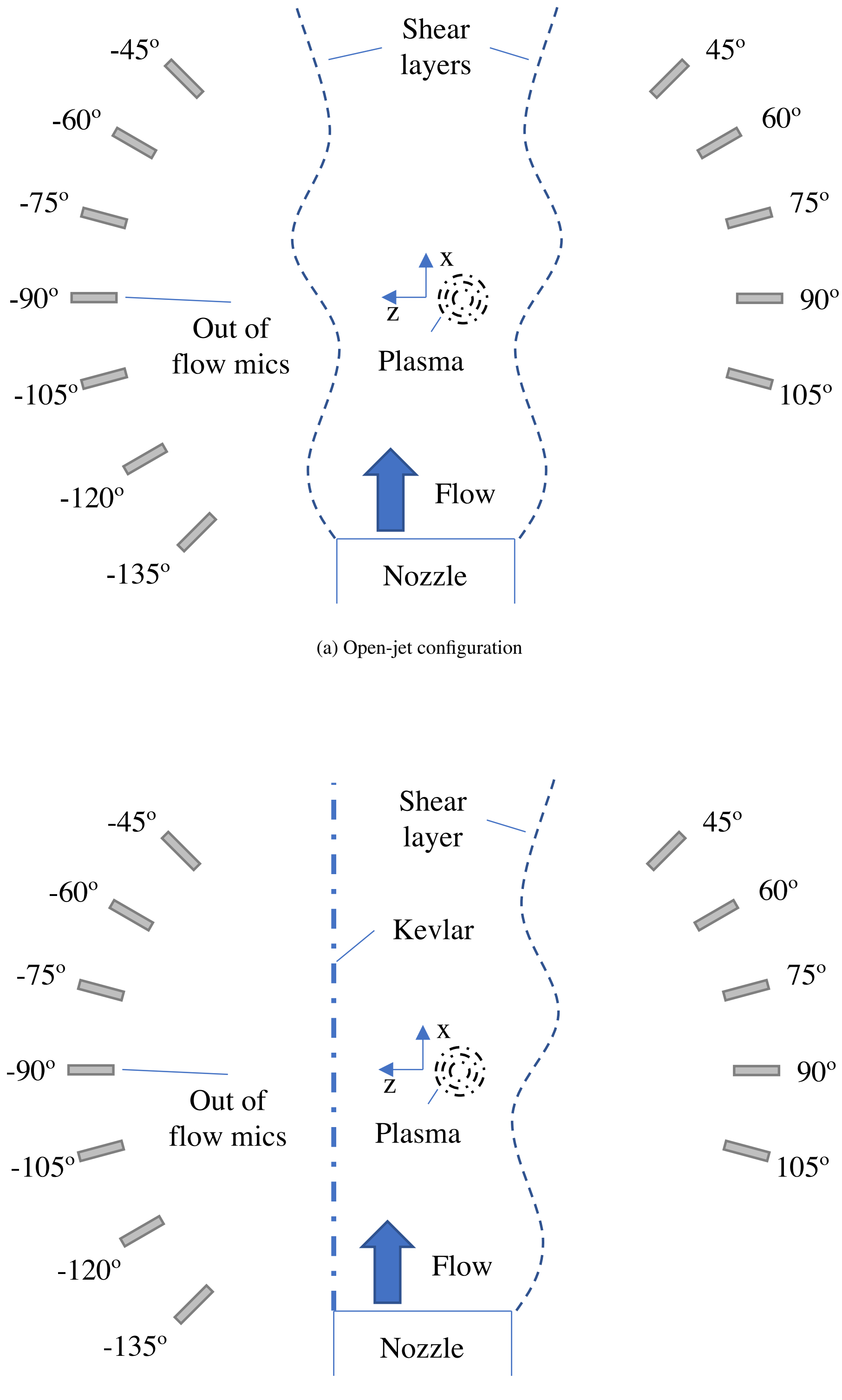

(a) Open-jet configuration

(b) Kevlar panel configuration

Fig. 1 Test section layout for acoustic measurements. Microphone locations are not to scale.

principle, the setup shown in Fig. 1b would be sufficient to assess the two interface types by comparing instrumentation on opposite sides of the test section. However, comparing the negative angle microphones in Fig. 1a to those in Fig. 1b while maintaining positive angle microphones as references mitigates the influence of minor impulse response differences between individual microphones. Assuming the microphone impulse response functions do not change between configurations, these divide out in the final calculation of relative changes when comparing a given microphone to itself. Note that the plasma source was not located at the origin of the coordinate system defining the microphone angles. For the data presented in this paper, it was located on the line between the $-90°$ and $90°$ microphones, offset 1 inch in the negative-z direction from the origin. This yielded a total error in labeled angles from the true angles of less than $1°$ for the worst case. Also, the microphones were not equidistant from the origin.

B. Data acquisition and processing

All microphone signals were routed through an analog bandpass filter system with a 150 Hz cut-on and 100 kHz cut-off. They were then discretized at a sampling rate of 250 kSamples/s. The q-switch from the laser and a photodetector signal were also routed (unfiltered) to the data system. Data were acquired continuously for 20 seconds, with a laser pulse repetition rate of 5 Hz. A 2 kHz phaseless digital highpass filter was applied to the data [26]. This filtering step removed some low frequency fluctuations in the data when test section flow was present, improving waveform analysis in the time domain.

A photodetector was incorporated into the test plan to allow for a more precise measurement of the source pulse initiation time, in case there was a delay between the trigger from the q-switch signal and source formation. It also allowed for the detection of misfires, where the laser might pulse but not form a source. This had been observed in some previous work [24]. After the test, it was found that for all inspected data the source formation rate was 100%, and the q-switch and photodetector yielded the same source formation time. The q-switch allowed individual pulse events to be parsed from continuous time records. For these measurement settings, each test configuration acquired either 100 or 101 pulses.

In an effort to improve the pulse-to-pulse alignment of the data referenced to the source formation time, a filtered reference microphone signal and the unfiltered photodetector signal were also routed to a National Instruments PXI-5122 card operating at 10 MSamples/s. Details of this process are presented in a previous version of this work [27], and have been removed here for brevity. The process described in the reference outputs microphone data oversampled to 1.25 MSamples/s and aligned to the clock of the higher sampling rate card.

It should be noted that for all of these plots, the pulses are not representative of the actual acoustic waveform, which likely has a shape closer to a true N-wave [28]. Rather, they are the pulse waveform distorted by the diaphragm, grid, and directivity response of the microphone, as well as by atmospheric attenuation and the bandpass filter applied to the microphone signal. The microphone grid in particular was observed to add significant distortion to the signal, as has been measured previously [24], and is a strong function of the microphone size and model characteristics. More accurate measurements of the waveform could require alternative measurement methods [29].

C. Data analysis

A variety of metrics have been used to characterize acoustic pulses propagating through turbulent media. Arrival time, rise time, peak pressure, and duration have all been considered parameters of interest. However, depending on the degree of waveform distortion these may be nontrivial to determine [30, 31]. The ensemble-averaged acoustic intensity in conjunction with the intensity autocorrelation function may be used to model pulse propagation through random media and isolate the effects of spread and wander [15, 16], although a different approach is used here.

1. Wander

In this work, wander is directly assessed by extracting the pulse-to-pulse arrival time. The arrival time, t_a, is computed as the first sample in a pulse block to surpass 5% of the peak absolute value of pressure in that block. This definition is found to identify arrival times extremely close to what might be determined from visual inspection of a given block, without falsely identifying a signal fluctuation early in the pulse block. This value is not a universal choice, and will depend on facility background noise levels.

2. Spread

Spread, or the change in signal shape from pulse-to-pulse, can be assessed by evaluating the frequency-domain behavior of the pulse blocks. Note that prior to any form of Fourier-based analysis, each pulse block is gated with a 600 μs long 25% Tukey window to remove any reflected or scattered signals from the data, reducing analysis to a single propagation path. It is assumed that the gating window, in addition to suppressing these additional signals, also sufficiently attenuates measurement noise such that it can be safely neglected in subsequent analysis. This is because the majority of the block length where the noise would exist is set to zero. The only remaining nonzero data are dominated by the acoustic pulse waveform. For consistency with the associated shielding study, blocks are zero-padded to interpolate frequency-domain data to a resolution of 61 Hz [20].

Following the general methodology of Pascioni et al. [32], the acoustic signal at microphone i due to an acoustic pulse is given as $Y_i(f) = H_i(f)\,X(f)$. X (frequency notation subsequently suppressed) is the spectral representation of the source signal while H_i is the complete combination of propagation path, interface, and frequency response effects, which influence microphone measurement Y_i. Unlike in the reference, no attempt is made to separate the components of H_i. It is assumed that most contributions to H_i from propagation through the test section potential core and the quiescent air outside of the test section are approximately invariant when compared between the open-jet and Kevlar configurations. Unlike with conventional system analysis, in this work, X is assumed to be deterministic (though unknown) while H_i is a random variable with mean and fluctuating components $\overline{H_i}$ and H_i', respectively.

As formulated here, any analysis of H_i will incorporate both the effects of spread and wander, as the randomization of t_a will add further variation to the phase angle of H_i beyond that due to the distortion from spread. As such, the pulse blocks are shifted in time by t_a prior to Fourier analysis. This shift is an attempt to remove the variation due to wander, to isolate the pulse spread in the frequency domain. The resultant formulation, where the arrival time of the pulse is defined as $t_a = 0$ in the shifted time domain, is given by

$$Y_{i,0} = H_{i,0}X = \left(\overline{H_{i,0}} + H_{i,0}'\right) X. \tag{1}$$

The sample mean of the shifted transfer function and input can be estimated by ensemble-averaging the shifted, transformed blocks,

$$\overline{Y_{i,0}} = E\left[\left(\overline{H_{i,0}} + H_{i,0}'\right) X\right] = \overline{H_{i,0}}X. \tag{2}$$

The sample variance can then be computed as

$$\overline{|Y_{i,0}'|^2} = E\left[\left(H_{i,0}'X\right)^* \left(H_{i,0}'X\right)\right] = E\left[\left(H_{i,0}'\right)^* \left(H_{i,0}'\right)\right]|X|^2 = \overline{|H_{i,0}'|^2}|X|^2 \tag{3}$$

with * denoting the complex conjugate operation. The influence of the source spectrum can be removed by computing the coefficient of variation. This is done by first computing the magnitude-squared of the mean,

$$|\overline{Y_{i,0}}|^2 = \left(\overline{H_{i,0}}X\right)^* \left(\overline{H_{i,0}}X\right) = |\overline{H_{i,0}}|^2|X|^2, \tag{4}$$

dividing the sample variance by this quantity, and taking the square root,

$$CV_i = \sqrt{\frac{\overline{|Y_{i,0}'|^2}}{|\overline{Y_{i,0}}|^2}} = \sqrt{\frac{\overline{|H_{i,0}'|^2}}{|\overline{H_{i,0}}|^2}}. \tag{5}$$

CV, or the coefficient of variation, is a normalization of the standard deviation that effectively removes the shape of the source spectrum, along with any instrumentation directivity and atmospheric attenuation effects, from analysis of the transfer function. Each microphone measurement is only compared to itself. CV should give a frequency-dependent measure of pulse spread.

3. Coherence

For this test, the coherence-squared between two microphones, $\gamma_{i,j}^2$, is representative of the spatiotemporal decorrelation experienced by the acoustic signal as it passes through a turbulent interface. For an ideal deterministic point source with a single, steady propagation path to each microphone, it should be identically unity. For an acoustic field that has been completely decorrelated, it should be zero. In conventional applications, coherence-based analysis will suffer from the mechanisms that drive both spread and wander. As such, in this work, it is computed without shifting the pulses in time. The definition used in this paper then becomes

$$\gamma_{i,j}^2 = \frac{E\left[Y_i{}^* Y_j\right] E\left[Y_i Y_j{}^*\right]}{E\left[Y_i{}^* Y_i\right] E\left[Y_j{}^* Y_j\right]} = \frac{E\left[(H_i X)^* \left(H_j X\right)\right] E\left[(H_i X)\left(H_j X\right)^*\right]}{E\left[(H_i X)^* (H_i X)\right] E\left[\left(H_j X\right)^* \left(H_j X\right)\right]} = \frac{|\overline{H_i^* H_j}|^2}{\overline{|H_i|^2}\,\overline{|H_j|^2}}. \tag{6}$$

On a frequency-by-frequency basis, the behavior of the coherence function can be further investigated by evaluating the normalized block-by-block terms that contribute to the cross-spectra between microphones,

$$C_{i,j} = \frac{Y_i^* Y_j}{\sqrt{E\left[Y_i{}^* Y_i\right] E\left[Y_j{}^* Y_j\right]}} = \frac{H_i^* H_j}{\sqrt{\overline{|H_i|^2}\,\overline{|H_j|^2}}}. \tag{7}$$

Note that for steady propagation from a single deterministic source, or when the variations in H_i and H_j are only in phase, the magnitude of $C_{i,j}$ should be unity.

4. Magnitude corrections

Without an accurate measurement of X, it is not possible to directly estimate H_i and therefore, not possible to compute a correction for it. However, if a consistent test setup is assumed, a relative magnitude correction between the Kevlar configuration and the open-jet configuration can be calculated. First, the mean-square magnitude for the microphone of interest in the Kevlar configuration is computed,

$$\overline{|Y_i^{Kev}|^2} = \overline{\left(H_i^{Kev} X\right)^* \left(H_i^{Kev} X\right)} = \overline{|H_i^{Kev}|^2}|X|^2. \tag{8}$$

This is repeated with a reference microphone, herein chosen to be the microphone at 90°. These values are then divided,

$$\frac{\overline{|Y_i^{Kev}|^2}}{\overline{|Y_{rm}^{Kev}|^2}} = \frac{\overline{|H_i^{Kev}|^2}}{\overline{|H_{rm}^{Kev}|^2}}. \tag{9}$$

This process is then repeated for the open-jet configuration, the results divided, and the square root taken to determine a relative transmission coefficient,

$$T_{rel} = \sqrt{\frac{\overline{|Y_i^{Kev}|^2}}{\overline{|Y_{rm}^{Kev}|^2}} \frac{\overline{|Y_{rm}^{Open}|^2}}{\overline{|Y_i^{Open}|^2}}} = \frac{\sqrt{\overline{|H_i^{Kev}|^2}}}{\sqrt{\overline{|H_i^{Open}|^2}}}. \tag{10}$$

A Kevlar panel measurement magnitude is thus divided by T_{rel} to recover the equivalent magnitude of an open-jet measurement for a given microphone location. Using the reference microphone to cancel X accounts for test-to-test variation in source characteristics between facility configuration changes. While these were not observed to be significant, their influence cannot be ruled out. Under the assumption that propagation magnitude effects do not change significantly for the reference microphone from configuration to configuration, the reference terms cancel, leaving the remaining terms to relate Kevlar and open-jet propagation to microphone i. The instrumentation response, instrumentation directivity, propagation through the test section potential core, and propagation through the quiescent air outside of the test section all cancel under the assumptions of this analysis.

The remaining contributions to T_{rel} are the change in interface from open-jet to Kevlar, the change in shear flow properties along the interface, and atmospheric attenuation. Atmospheric attenuation should be considered due to changes in thermodynamic properties across configuration changes. This can be determined by computing the atmospheric attenuation coefficient [33] and then using Amiet's method to determine the propagation path both in the test section flow and the surrounding chamber [5]. The test section propagation distance is modified with a Galilean transformation to account for convective effects, and then added to the chamber propagation distance to get an effective propagation distance, which is used to compute total attenuation. The total attenuation is then applied as a gain to the microphone spectra Y_i and Y_{rm}.

A previous version of this work attempted to construct phase corrections relating Kevlar to open-jet propagation [27]. However, as will be shown in a subsequent section of this article, the variability in the open-jet data at higher frequencies is extreme. Attempting to use such data with the proposed phase correction method likely yields erroneous results. A different technique using a different test setup would be required to adequately assess the influence of a Kevlar panel on the phase angle of a measured acoustic source.

5. Autospectra and background noise

The autospectra of the acoustic pulses are computed by the traditional method of ensemble averaging the square magnitude of the Fourier transform of each pulse block. This does not provide the noise rejection benefit of ensemble averaging the pulses themselves, but makes the estimate insensitive to wander and less sensitive to spread. These calculations are done without an additional window function as the blocks have already been gated with a Tukey window. The background noise characteristics of the Kevlar panel relative to the open-jet configuration are calculated from data acquired with the laser turned off. These calculations are performed with the standard RMS-average power approach, or Welch's method, using 75% overlap with a Hann window of 4096 points on the 250 kSamples/sec data.

IV. Results and Discussion

Results of the analysis methods given in the previous section are now presented. However, prior to delving into these quantitative terms, a brief qualitative discussion of the data is warranted. Individual, source-synchronized pulse waveforms are overlain in Fig. 2 for the $-45°$ microphone with no flow and at Mach 0.17 for both configurations. This microphone is chosen as it should experience the greatest influence of the turbulent shear layers shown in the setup. For clarity, only the first seven waveforms in each acquisition are shown. With no flow, as expected, the waveforms align extremely well. The Kevlar shows a slightly greater t_a than the open-jet configuration, but this is accounted for by the difference in the speed of sound from one test to the next, and illustrated with an overlay of Amiet's propagation time prediction. As might be expected, the Kevlar panel does not appear to introduce a significant delay in propagation time when compared to the open-jet. The waveform magnitude is slightly reduced when comparing the Kevlar to the open-jet. With test section flow at Mach 0.17, again the Kevlar shows a slightly greater t_a than the open-jet configuration, which is again accounted for by differences in the speed of sound. The variability of the waveform magnitude and arrival time of the waveform with the Kevlar is much lower than with the open-jet configuration. The open-jet waveforms also appear to suffer significantly more distortion of shape.

As an aside, Fig. 2 is a helpful illustration of the contribution of both wander and spread to the blurring seen due to coherence loss in microphone phased array processing that was mentioned previously. If data are shifted using Amiet's propagation calculation in time (or the associated phase shift in frequency) for a given grid point in a beam map, the pulses will not align properly from microphone to microphone. Instead, peaks of the waveform from one microphone will line up with off-peak parts of the waveform at a different microphone. Waveform distortion from spread further contributes to this error. Through averaging, this will attenuate the beamformer output at the true source location. However, it can also increase the output at other locations in space. The beam map becomes spatially "smeared."

A. Wander

Wander is herein assessed by comparing the standard deviation of the arrival time, t_a, between test section configurations for all the measured angles and Mach numbers. This is plotted in Fig. 3. The wander with no flow is approximately the same between configurations, and is likely a combination of small fluctuations in chamber properties and the temporal resolution of the pulse measurements. When the test section is operated at a nonzero Mach number, the open-jet configuration wander significantly surpasses that of the Kevlar panel for all Mach numbers and angles. For both configurations, a minimum appears at the upstream angles, progressively increasing in the downstream direction. The Kevlar wander is approximately the same for both Mach 0.13 and 0.17. With rare exception, the open-jet wander continues to increase at all angles with increasing Mach number.

B. Spread

Spread, as discussed previously, is assessed by evaluating the coefficient of variation of the spectral data after shifting the individual pulse blocks to mitigate the phase variations due to wander. This spread metric is plotted in Figs. 4 and 5. Frequency plot bounds are selected with the digital highpass filter cut-on as the lower limit and the analog lowpass filter cut-off as the upper limit. As with wander, the spread of the pulses with no flow is approximately the same

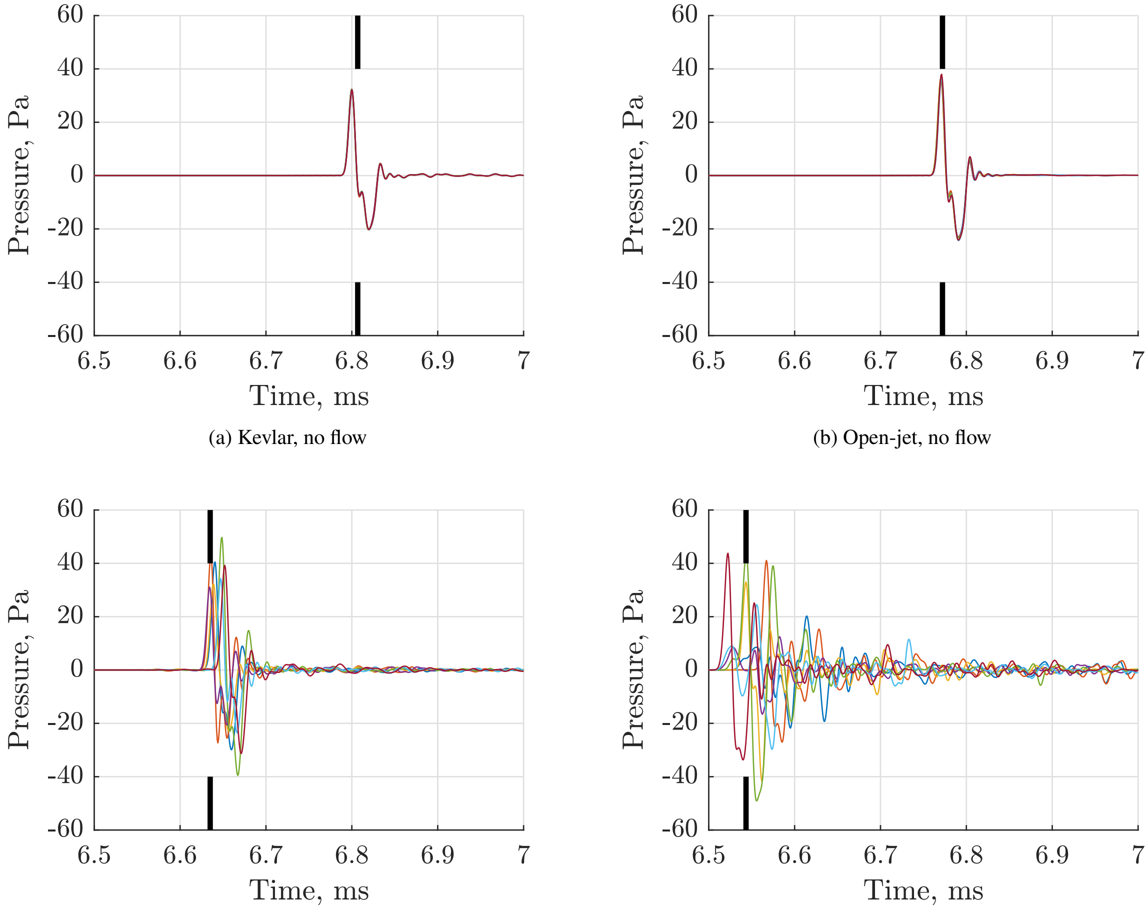

(a) Kevlar, no flow
(b) Open-jet, no flow
(c) Kevlar, Mach 0.17
(d) Open-jet, Mach 0.17

Fig. 2 First seven waveforms acquired in a given test for varying configuration and Mach number, as measured at the $-45°$ microphone. The vertical, broken black line denotes the propagation time prediction from Amiet's method.

between configurations. When the test section is operated at a nonzero Mach number, the open-jet configuration spread significantly surpasses that of the Kevlar panel for all Mach numbers and angles. Spread increases as a function of frequency in all the data. Individual peaks appear in some spread calculations, but no attempt is made to assign physical meaning to these peaks beyond general data trends.

At its worst, the Kevlar panel spread approaches a CV of 0.5 at the $-45°$ microphone for a Mach number of 0.17. These low CV values suggest that most propagation through the Kevlar panel is dominated by mean effects once wander has been removed, rather than by fluctuating effects. Conversely, the spread of the open-jet data always reaches unity at high frequencies for a Mach number of 0.17. Additionally, at the downstream angles of $-60°$ and $-45°$, CV reaches values of 10 or greater at high frequencies, and surpasses unity below 20 kHz. This suggests that, at these downstream angles, a signal with high frequency content is dominated by fluctuating effects once wander has been removed, rather than by mean effects. Thus, for the Kevlar panel, weak scattering may be a safe assumption. For the

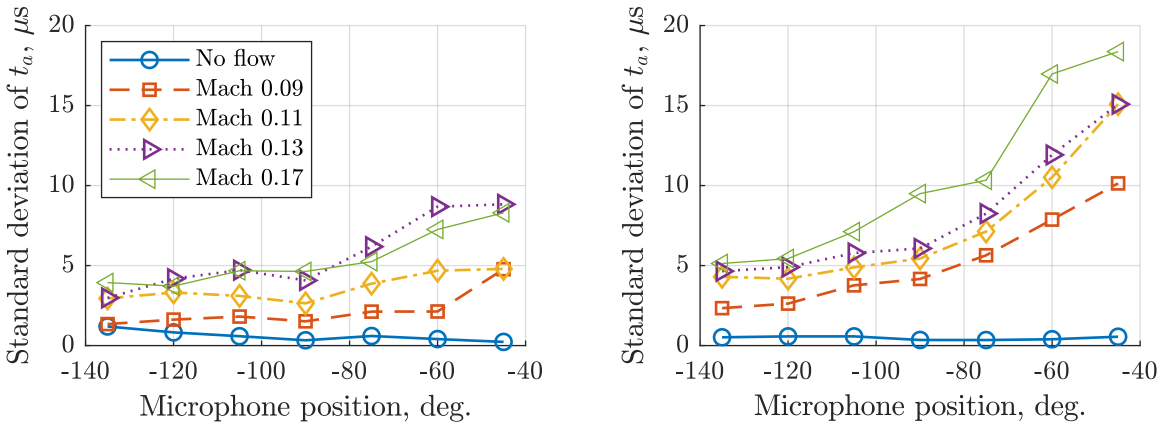

(a) Kevlar (b) Open-jet

Fig. 3 Comparison of standard deviation of arrival time, t_a, between test section configurations.

open-jet configuration, downstream propagation at higher test section Mach numbers appears to experience strong scattering.

C. Coherence

The coherence between channels is now considered. The microphone at −90° is used as the reference microphone for coherence calculations, and all other microphones on the same side of the Kevlar panel or free shear layer are analyzed. The coherence plots are shown in Figs. 6 and 7, sorted by downstream and upstream angles, respectively. Coherence is not quite unity as it would be under ideal no flow conditions. At high frequencies, there is a minor roll-off. This may be due to small fluctuations in thermodynamic properties, or possibly due to minor unsteady free convection in the facility.

As with the other unsteady metrics, for all nonzero flow speeds, the Kevlar panel shows improved behavior when compared to the open-jet configuration. Interestingly, the Kevlar shows improved coherence behavior when comparing the Mach 0.13 data to the Mach 0.17 data. This would appear to be in agreement with the wander data shown in Fig. 3a, where, for many angles, the wander is nearly the same when comparing those Mach numbers. If coherence roughly trends with wander for the Kevlar panel, this might further support a weak scattering assumption for this test configuration. The open-jet data show far more coherence reduction for a given angle and Mach number, dropping as low as $\gamma^2 = 0.2$ at 10 kHz for the −45° microphone at Mach 0.17.

The behavior of the coherence can be further investigated by evaluating the metric C as defined in Eq. 7. This metric is a normalized representation of the elements that average into a cross-spectrum, and thus the coherence function. The real and imaginary components of C calculated between the −45° and −90° microphones at Mach 0.17 are plotted in Fig. 8, where each point represents the result from an individual pulse. This type of plot has been used previously to characterize the data spread in cross-spectral calculations for microphone phased arrays [34]. The subfigures overlay C

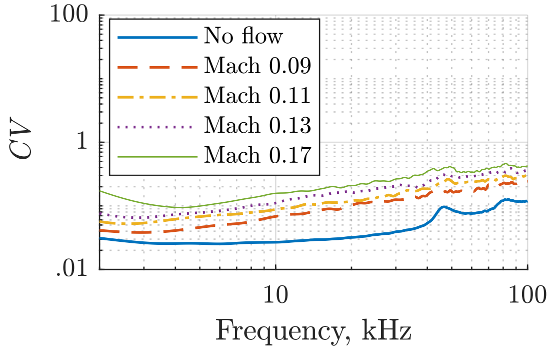

(a) Kevlar, −45° mic

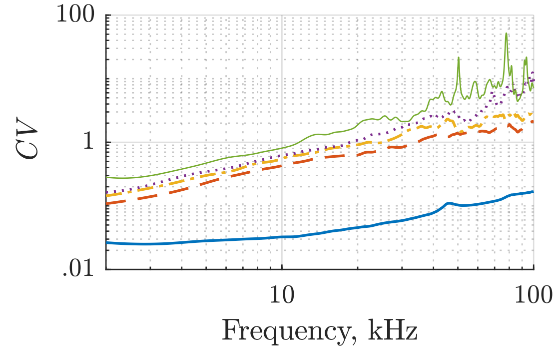

(b) Open-jet, −45° mic

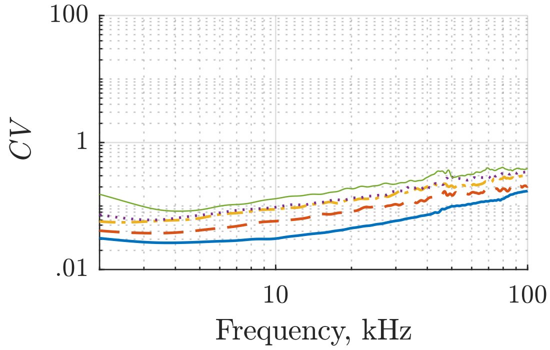

(c) Kevlar, −60° mic

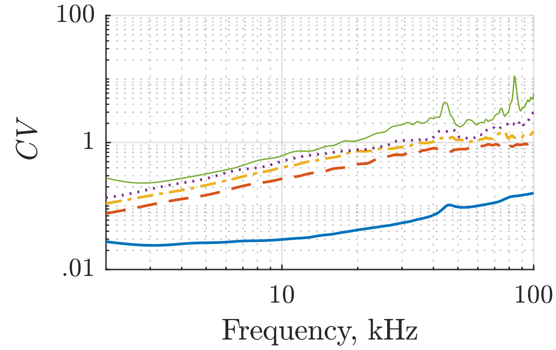

(d) Open-jet, −60° mic

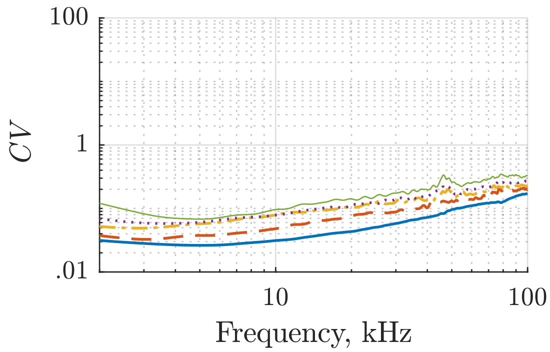

(e) Kevlar, −75° mic

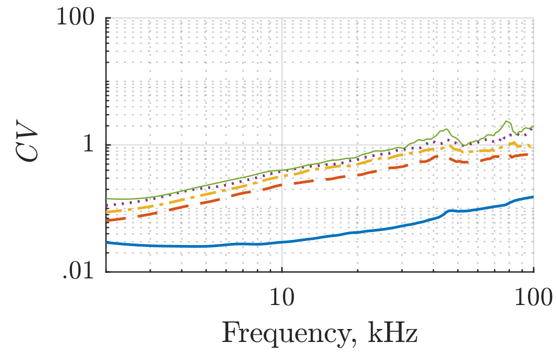

(f) Open-jet, −75° mic

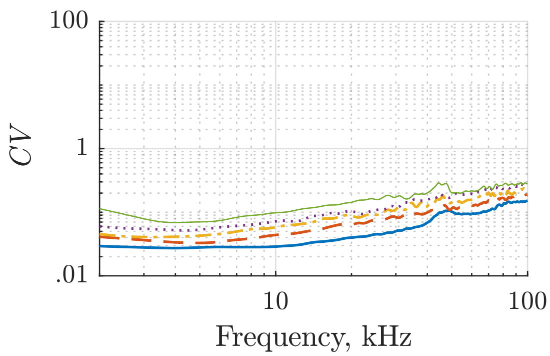

(g) Kevlar, −90° mic

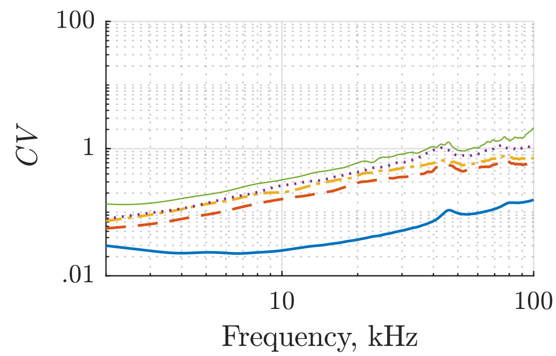

(h) Open-jet, −90° mic

Fig. 4 Comparison of CV as a function of frequency between test section configurations for downstream angles.

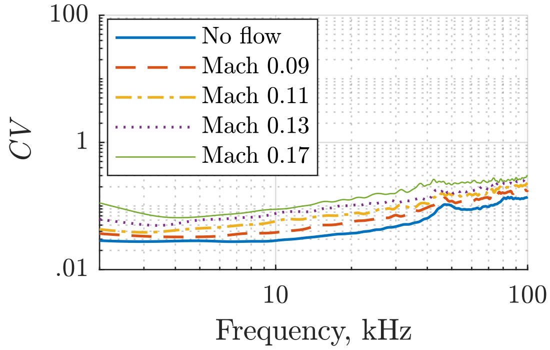

(a) Kevlar, −105° mic

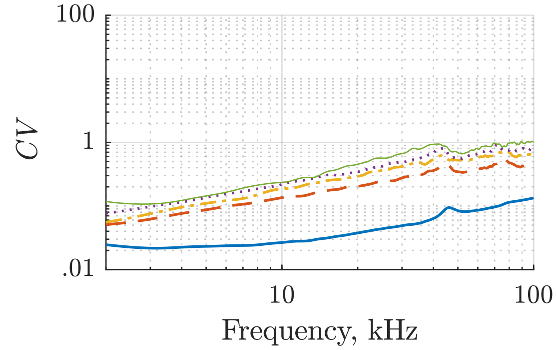

(b) Open-jet, −105° mic

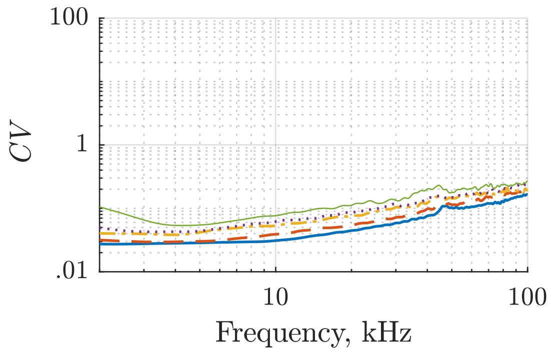

(c) Kevlar, −120° mic

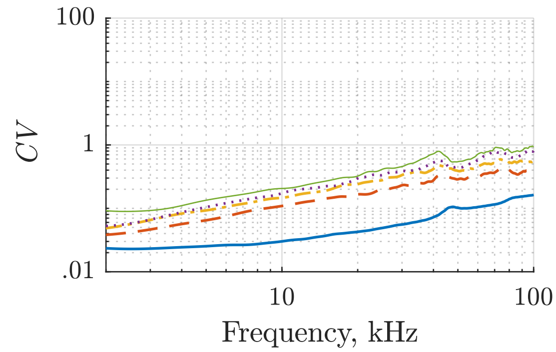

(d) Open-jet, −120° mic

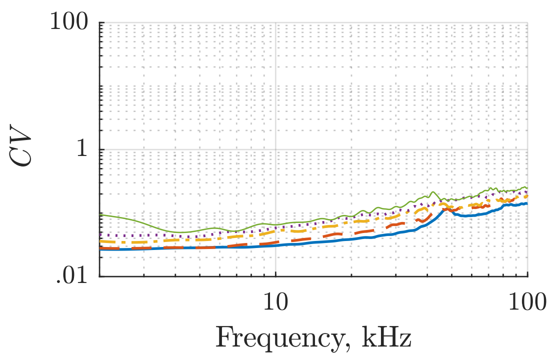

(e) Kevlar, −135° mic

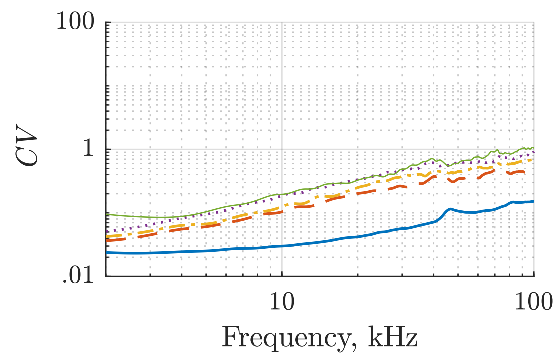

(f) Open-jet, −135° mic

Fig. 5 Comparison of CV as a function of frequency between test section configurations for upstream angles.

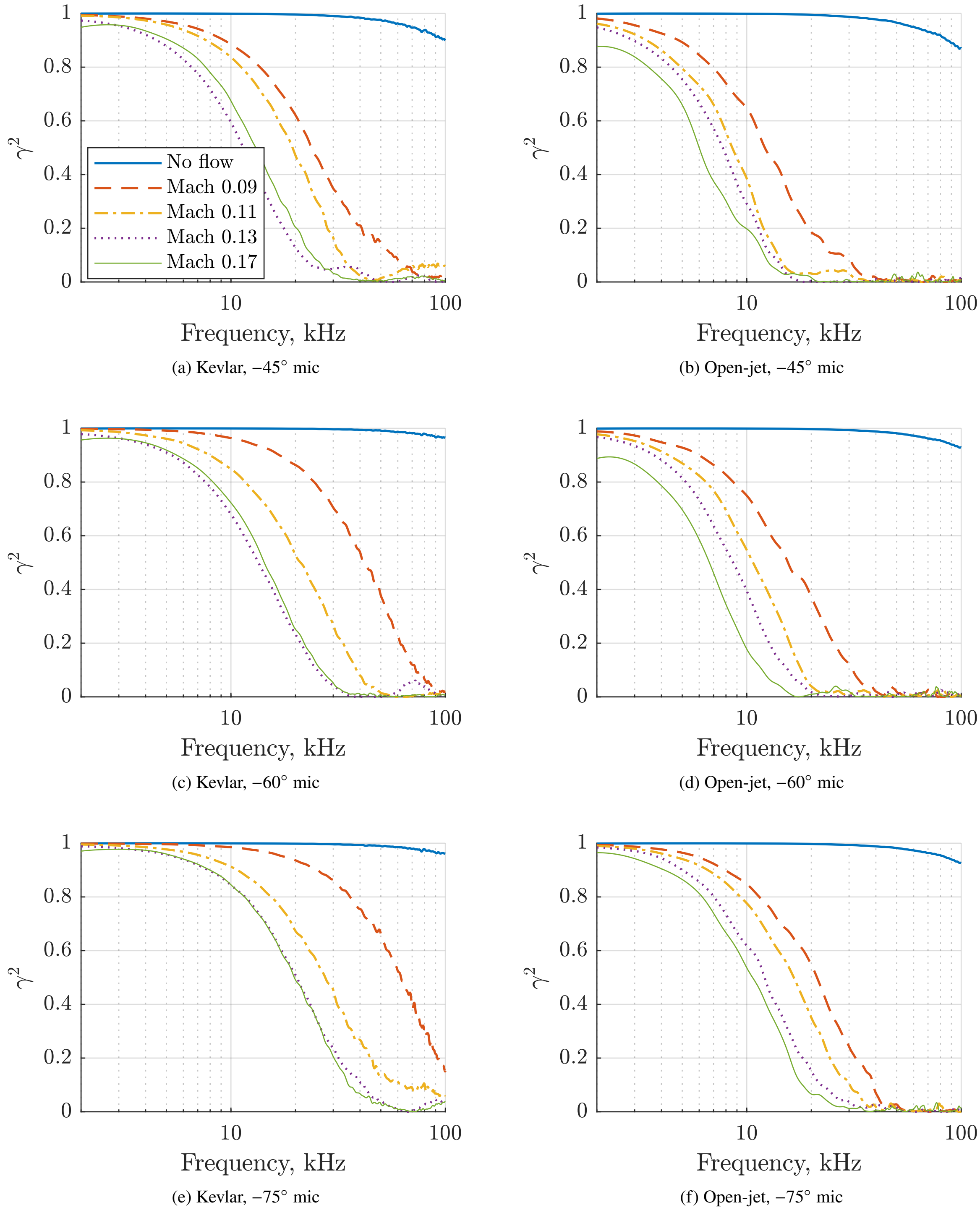

(a) Kevlar, −45° mic
(b) Open-jet, −45° mic
(c) Kevlar, −60° mic
(d) Open-jet, −60° mic
(e) Kevlar, −75° mic
(f) Open-jet, −75° mic

Fig. 6 Comparison of γ^2 as a function of frequency between test section configurations for downstream angles. The reference microphone is at −90°.

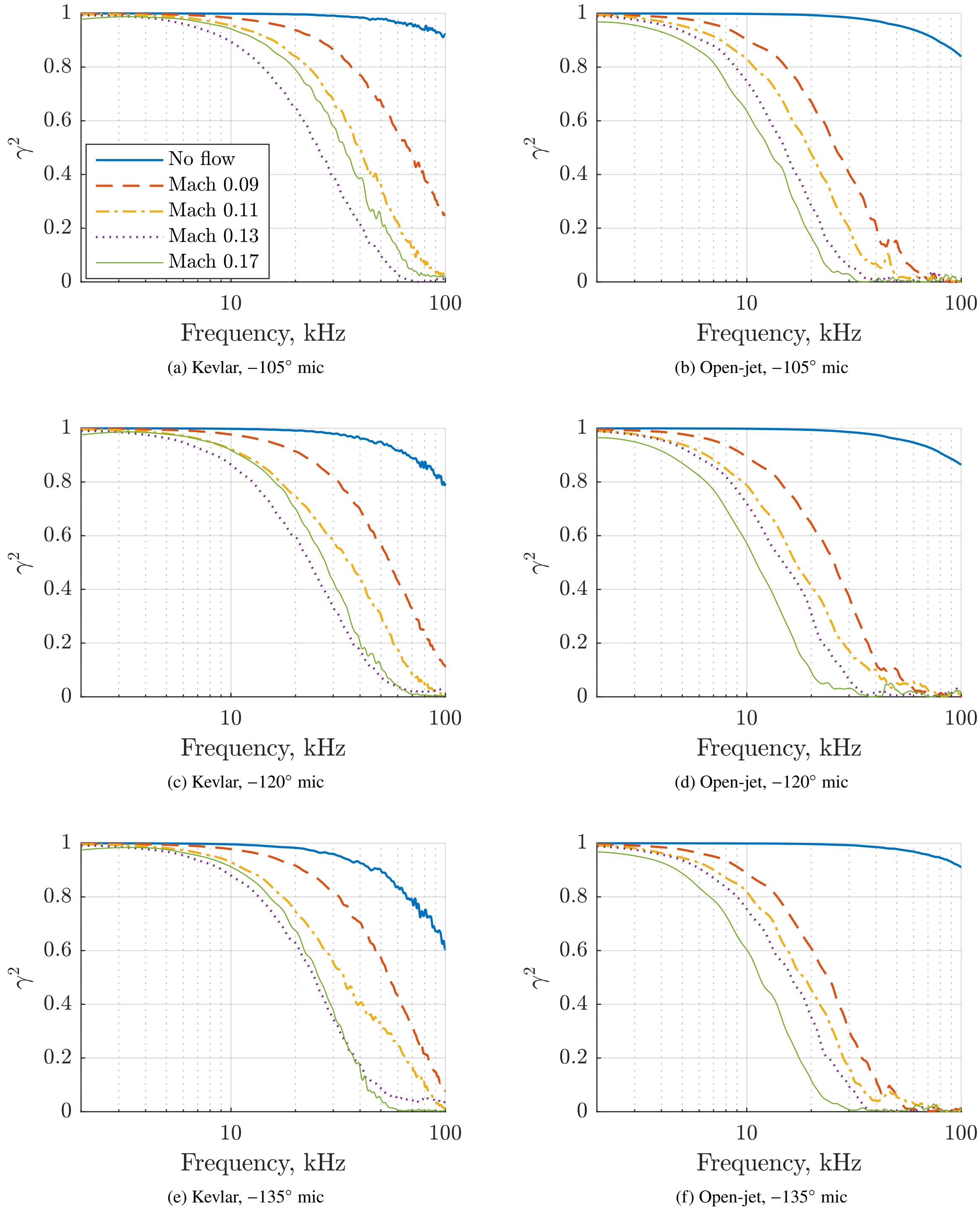

(a) Kevlar, −105° mic

(b) Open-jet, −105° mic

(c) Kevlar, −120° mic

(d) Open-jet, −120° mic

(e) Kevlar, −135° mic

(f) Open-jet, −135° mic

Fig. 7 Comparison of γ^2 as a function of frequency between test section configurations for upstream angles. The reference microphone is at −90°.

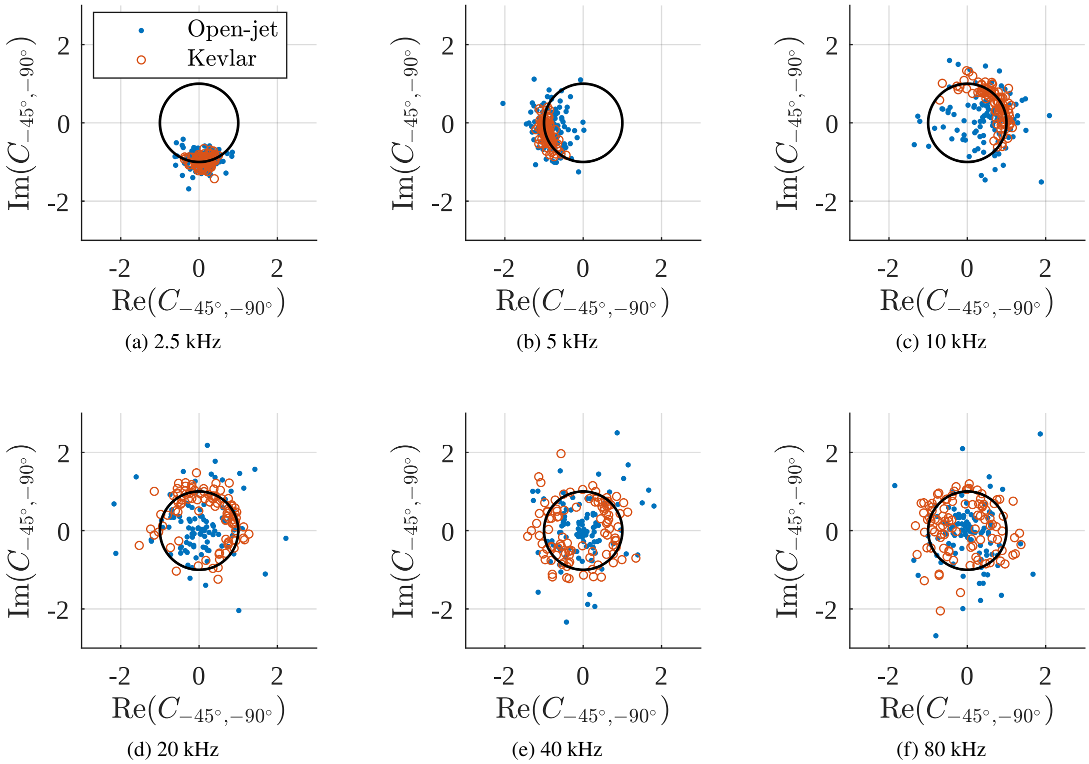

(a) 2.5 kHz (b) 5 kHz (c) 10 kHz

(d) 20 kHz (e) 40 kHz (f) 80 kHz

Fig. 8 Evaluation of $C_{-45^\circ,-90^\circ}$ for several frequencies at Mach 0.17.

for both Kevlar and open-jet tests, along with the unit circle, for a range of frequencies. To reiterate, C should have a magnitude of unity when propagation is steady from a single deterministic source, as well as when all variation in propagation is due to randomized phase shifts. Purely phase-related variation would suggest that the propagation unsteadiness is dominated by wander, or changes in propagation time, and is thus weak scattering as defined previously.

At low frequencies, shown in Figs. 8a and 8b, the Kevlar and open-jet configurations show similar character. For the most part, C is concentrated on the unit circle for both, though the open-jet data show slightly more magnitude variation. Conventional averaging of these cross-spectral terms (averaging real and imaginary parts independently) would yield the desired results of each point cloud centroid.

At midrange frequencies, shown in Figs. 8c and 8d, the behavior of the open-jet data diverges from the behavior of the Kevlar data. C for the Kevlar continues to concentrate around the unit circle, but C for the open-jet begins to see significant magnitude scatter. At 10 kHz, the average of the Kevlar C is not nearly as degraded in magnitude as the average of the open-jet C. This is also shown in the significant difference in coherence values at 10 kHz in Figs. 6a (≈ 0.7) and 6b (≈ 0.2) for the corresponding data. At 20 kHz, the open-jet C is effectively zero mean. The Kevlar data, when averaged conventionally, is close to zero mean. However, the structure of the Kevlar data suggests its magnitude degradation may be correctable. For one, conventional averaging could be replaced with magnitude and phase averaging. This would collapse the average of C to the proper phase angle without a loss in magnitude. Unfortunately, such averaging will not fully suppress noise that is uncorrelated between the two channels contributing to C, nor will it suppress cross-terms between uncorrelated noise sources. As such, magnitude and phase averaging is unsuitable for many aeroacoustic tests. The more general alternative is to introduce an in situ calibration reference as has been demonstrated in previous work [17, 34].

The trends from the midrange frequencies continue at the high frequencies plotted in Figs. 8e and 8f. The distribution of phase angles for the Kevlar data is sufficiently broad that phase averaging is now meaningless. However, the magnitude spread has still not approached zero mean, so a calibration reference might still be successful in correcting the Kevlar C. The scatter for the open-jet C continues to behave as it did at 20 kHz.

D. Magnitude corrections

The computed correction factors are shown in Fig. 9. The magnitude corrections show significant fluctuation. This has been reported previously with other wind tunnel installations [3], though much cleaner results with a pulsed laser source have also been obtained [32]. Some of this fluctuation may be attributed to the structural response of the Kevlar panel itself to both the flow loading and the acoustic wave. Comparing Fig. 2a to Fig. 2b, it is evident that some ringing is present in the signal after the initial pulse arrival for the Kevlar configuration and that this ringing does not appear to change from block to block. This is not the case for the open-jet configuration, and suggests a deterministic component of the Kevlar installation. Doppler shift due to source motion may also generate some ripple in the curves at higher Mach numbers, and is discussed in the next section.

Considering overall trends and neglecting these peaks and troughs in the plots, the magnitude correction is slightly lower than in other references for their reported frequency ranges. While other work has reported a velocity dependence in the magnitude correction factor for Kevlar, it is not observed here. This is likely because in this work the Kevlar is referenced to a free shear layer, which already has a velocity-dependent correction factor [5]. The overall relative magnitude correction for the Kevlar does not show a strong angle dependence in trends, indicating that whatever directionality is present, it is small and behaves the same as the free shear layer directionality.

E. Autospectra and Background Noise

Autospectral densities of the signal are shown in Fig. 10 for a range of Mach numbers at an upstream, central, and downstream angle. For autospectral densities, the microphone directivity and actuator response do not cancel in the calculations. Therefore, these corrections [35] are applied to the data in addition to atmospheric attenuation. Note that these corrections are based on smoothed approximations, and do not completely remove instrumentation effects. In general, the source appears to behave as a moving point source, matching the observations made in the companion shielding test [20]. There is a positive Doppler frequency shift in the downstream direction, the direction of source

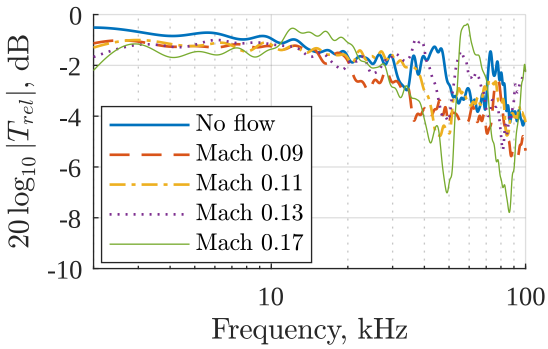

(a) −45° mic

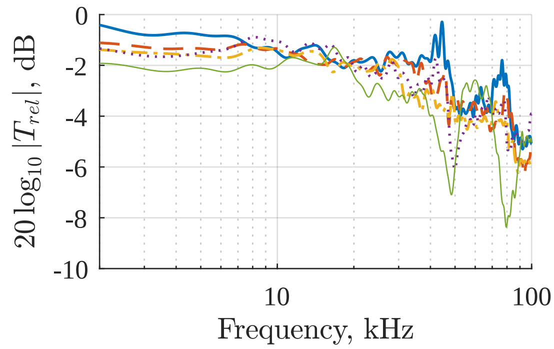

(b) −60° mic

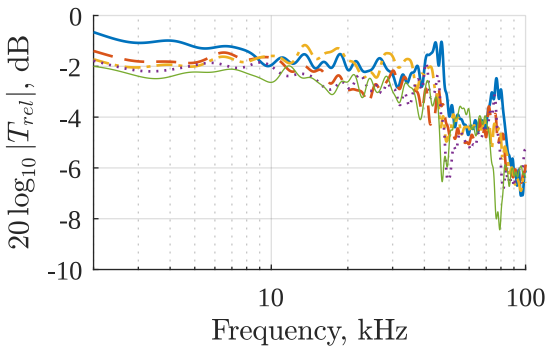

(c) −75° mic

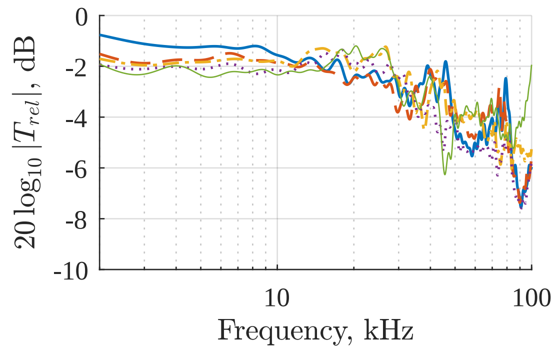

(d) −90° mic

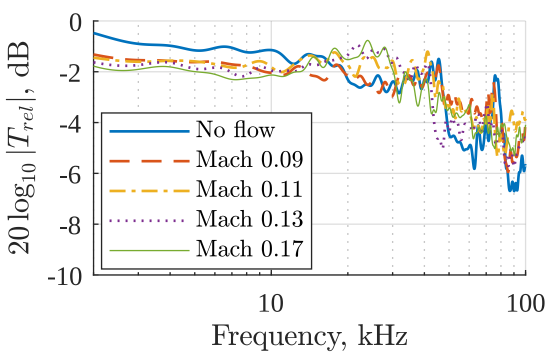

(e) −105° mic

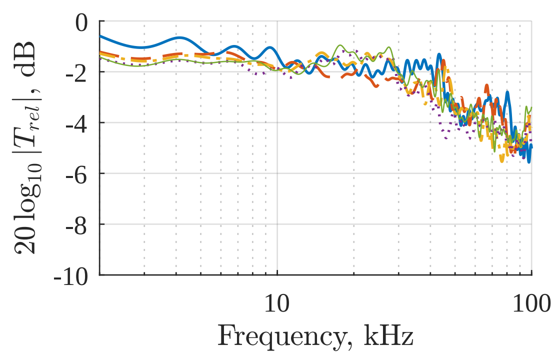

(f) −120° mic

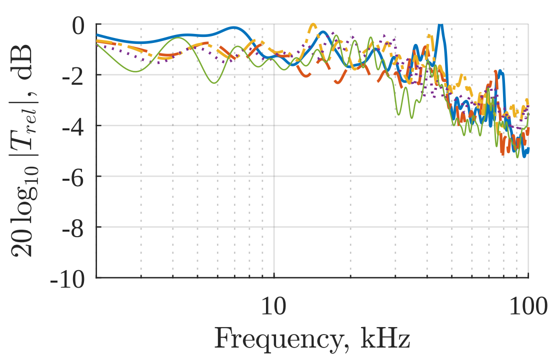

(g) −135° mic

Fig. 9 Comparison of T_{rel} as a function of frequency and Mach number.

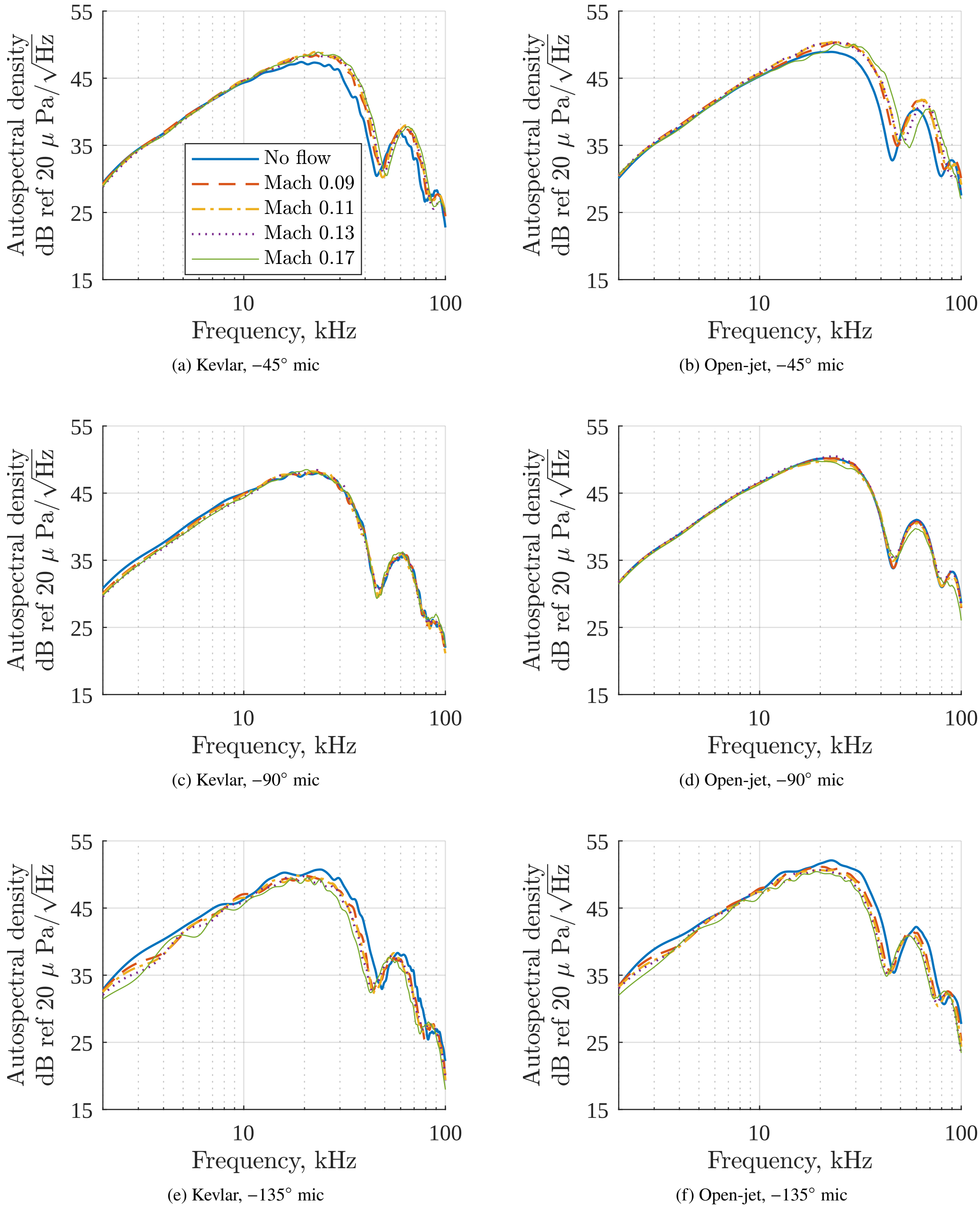

(a) Kevlar, −45° mic
(b) Open-jet, −45° mic
(c) Kevlar, −90° mic
(d) Open-jet, −90° mic
(e) Kevlar, −135° mic
(f) Open-jet, −135° mic

Fig. 10 Corrected autospectral densities of pulse waveforms for varying angle and Mach number.

motion, and an increase in level with increasing Mach number. In the upstream direction, there is a negative Doppler frequency shift and a reduction in level with increasing Mach number. This agrees with the existing model for the acoustic source [22].

The spectra for the far downstream angle of −45° in the open-jet configuration appears to behave more erratically as compared to the Kevlar at the equivalent angle at Mach 0.17, when considering the frequency and magnitude of the dominant trough and secondary peak in the spectral shape. Similarly, this open-jet angle is more erratic than the other angles for both configurations. One possible cause of this, though unprovable with the current data, is that the turbulence in the free shear layer is sufficiently strong that the additional Doppler influence from eddy scattering is further spreading the spectrum [36]. This spreading affects the alignment of the spectra in the correction process from the previous section. When inspected visually, this misalignment of the secondary peak in the spectrum appears to drive the large peak and trough structures in the T_{rel} plots for downstream angles in Fig. 9. This Doppler misalignment does not appear in the upstream angle autospectra in Fig. 10.

Finally, (uncorrected) background noise autospectral densities for the two configurations are shown in Fig. 11. Only one angle is plotted, as all angles show approximately the same behavior. These data were acquired by simply turning the laser system off for a given test condition with both configurations. Note that the measurement system noise floor is evident in almost all datasets at some frequencies, and completely dominates the no flow data. This is because the data acquisition system ranges and amplifier gains were set to acquire the laser pulse signal, not to measure an accurate facility acoustic noise floor. The gains could be increased by another 20 dB for a pure background noise measurement. Also, the noise floor levels shown in these plots are not representative of the noise floor in the laser pulse analyses. As mentioned in the discussion of the pulse spread, the gating process applied to the pulse data significantly reduces background noise power in computed spectra.

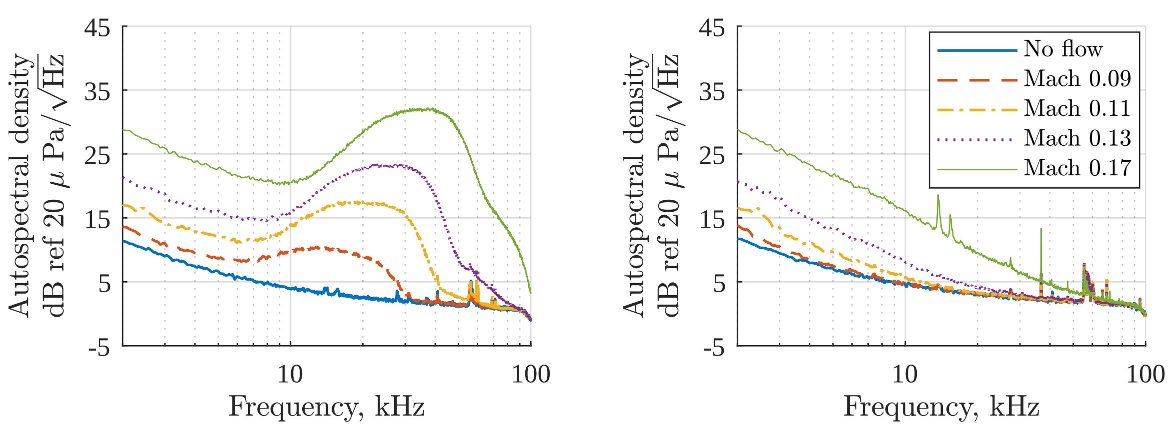

(a) Kevlar, −60° mic

(b) Open-jet, −60° mic

Fig. 11 Background autospectral densities of the two configurations as a function of Mach number.

This comparison is the only one where the open-jet configuration shows a clear advantage when compared to the Kevlar panel when considering aeroacoustic measurement interests. At lower frequencies, noise levels from the Kevlar and open-jet configurations are similar, and both approximately the same at 3 kHz for Mach 0.17. However, at higher frequencies, the Kevlar panel data dramatically diverge from the open-jet data. At 10 kHz, the Kevlar data are approximately 5 dB above the open-jet data. The difference peaks at 40 kHz, with the background noise produced by the Kevlar configuration over 25 dB higher than that produced by the open-jet configuration. Depending on the nature of a given test, the Kevlar panel could prove problematic when attempting to measure a low level acoustic source.

V. Summary and Recommendations

A test comparing the unsteady propagation characteristics of an acoustic pulse in two different configurations of aeroacoustic wind tunnels is presented. The test compared the open-jet configuration with the Kevlar wall configuration, using a laser-generated acoustic point source. The pulsed source allows for the isolation of the direct propagation path through a gating process, and can be studied in terms of wander and spread. Metrics for these based on the current test are proposed, along with potential correction techniques.

By all proposed assessment metrics, the Kevlar panel configuration experiences far less unsteady influence on propagation from the source to the microphones. The spread of the pulses, or waveform distortion, is minimal with the Kevlar configuration, particularly when compared to the open-jet configuration. The wander, or variation in pulse arrival time, is also less with the Kevlar panel than with the open-jet configuration. These two characteristics drive the coherence behavior of the two configurations, where the Kevlar panel shows reduced decorrelation effects when compared to an open-jet configuration.

Relative corrections between the configurations are proposed and calculated. These corrections (as calculated in this test) are influenced by a possible structural response of the Kevlar panel in combination with Doppler effects, making true quantitative analysis difficult. However, the data allow for qualitative discussion of the corrections. The overall magnitude correction trends with previous work, although the specific levels may be in disagreement. The magnitude correction shows little dependence on directivity and Mach number. This is likely because the magnitude correction is relative, so these directivity effects are common between the open-jet and Kevlar panel configurations. Individual spectra confirm the Doppler behavior of the signal, and show that the Kevlar panel generates significantly more background noise than the open-jet at higher frequencies.

For a future test, the choice between Kevlar and open-jet configurations must be determined by the test requirements. Previous work has repeatedly shown that if a wind tunnel model will generate a significant amount of lift, Kevlar walls are far preferable to an open-jet. However, when high lift is not a concern, the source and measurement plan of interest should drive the decision process. For a measurement scheme where coherence is critical, Kevlar appears to be the superior choice. All of the unsteadiness metrics are far lower for the Kevlar panel than they are for the open-jet configuration. This would suggest that microphone phased arrays, for example, would benefit more from the Kevlar configuration than the open-jet configuration. Similarly, a test plan with distributed coherent sources should consider utilizing Kevlar walls. Conversely, if an aeroacoustic source of interest is particularly quiet, an open-jet configuration may be considered. The background noise production of the Kevlar is sufficiently high such that it could completely mask a 40 kHz source that is perfectly observable otherwise. The extent of spatial coherence for the source should still be considered here. A quiet source measurement, which either has a large amount of source spatial coherence or is being acquired by a microphone phased array with large microphone spacings, will prove challenging in either configuration.

Acknowledgments

The authors would like to acknowledge Dr. Russell Thomas of the NASA Langley Research Center for leading the overall task and NASA contribution to the NATO effort, as well as funding by the NASA Advanced Air Transport Technology Project.

References

[1] Soderman, P. T., and Allen, C. S., "Microphone Measurements In and Out of Airstream," *Aeroacoustic Measurements*, edited by T. J. Mueller, Springer-Verlag, Berlin, Heidelberg, New York, 2002, pp. 1–61.

[2] Remillieux, M. C., Camargo, H. E., Ravetta, P. A., Burdisso, R. A., and Ng, W. F., "Novel Kevlar-Walled Wind Tunnel for Aeroacoustic Testing of a Landing Gear," *AIAA Journal*, Vol. 46, No. 7, 2008, pp. 1631–1639. doi:https://doi.org/10.2514/1.33082.

[3] Devenport, W. J., Burdisso, R. A., Borgoltz, A., Ravetta, P. A., Barone, M. F., Brown, K. A., and Morton, M. A., "The Kevlar-walled anechoic wind tunnel," *Journal of Sound and Vibration*, Vol. 332, No. 17, 2013, pp. 3971–3991. doi: https://doi.org/10.1016/j.jsv.2013.02.043.

[4] Miles, J. W., "On the Reflection of Sound at an Interface of Relative Motion," *The Journal of the Acoustical Society of America*, Vol. 29, No. 2, 1957, pp. 226–228. doi:https://doi.org/10.1121/1.1908836.

[5] Amiet, R. K., "Refraction of Sound by a Shear Layer," *Journal of Sound and Vibration*, Vol. 58, No. 4, 1978, pp. 467–482. doi:https://doi.org/10.1016/0022-460X(78)90353-X.

[6] Ostashev, V. E., and Wilson, D. K., "Random inhomogeneities in a moving medium and scattering of sound," *Acoustics in Moving Inhomogeneous Media*, CRC Press, Taylor & Francis Group, LLC, 2016, pp. 187–222.

[7] Michel, U., "On the systematic error in measurements of jet noise flight effects using open jet wind tunnels," *21st AIAA/CEAS Aeroacoustics Conference*, AIAA 2015-2996, Dallas, Texas, 22–26 June 2015. doi:https://doi.org/10.2514/6.2015-2996.

[8] Dougherty, R. P., "Turbulent Decorrelation of Aeroacoustic Phased Arrays: Lessons from Atmospheric Science and

Astronomy," *9th AIAA/CEAS Aeroacoustics Conference*, AIAA 2003-3200, Hilton Head, South Carolina, 12–14 May 2003. doi:https://doi.org/10.2514/6.2003-3200.

[9] Pires, L. S., Dougherty, R. P., Gerges, S. N. Y., and Catalano, F., "Predicting Turbulent Decorrelation in Acoustic Phased Array," *50th AIAA Aerospace Sciences Meeting*, AIAA 2012-0387, Nashville, Tennessee, 9–12 January 2012. doi:https://doi.org/10.2514/6.2012-387.

[10] Ernst, D., Spehr, C., and Berkefeld, T., "Decorrelation of Acoustic Wave Propagation through the Shear Layer in Open Jet Wind Tunnel," *21st AIAA/CEAS Aeroacoustics Conference*, AIAA 2015-2976, Dallas, Texas, 22–26 June 2015. doi:https://doi.org/10.2514/6.2015-2976.

[11] Ross, R., "Spectral Broadening Effects in Open Wind Tunnels in Relation to Noise Assessment," *AIAA Journal*, Vol. 19, No. 5, 1981, pp. 567–572. doi:https://doi.org/10.2514/3.50978.

[12] McAlpine, A., and Tester, B. J., "Spectral Broadening of Tonal Sound Propagating Through an Axisymmetric Turbulent Shear Layer," *AIAA Journal*, Vol. 58, No. 3, 2020, pp. 1093–1106. doi:https://doi.org/10.2514/1.J058000.

[13] Bahr, C. J., and Horne, W. C., "Subspace-based background subtraction applied to aeroacoustic wind tunnel testing," *International Journal of Aeroacoustics*, Vol. 16, No. 4–5, 2017, pp. 299–325. doi:https://doi.org/10.1177/1475472X17718885.

[14] Hutcheson, F. V., Spalt, T. B., Brooks, T. F., and Plassman, G. E., "Airframe noise from a hybrid wing body aircraft configuration," *International Journal of Aeroacoustics*, Vol. 16, No. 7–8, 2017, pp. 540–562. doi:https://doi.org/10.1177/1475472X17727609.

[15] Liu, C. H., and Yeh, K. C., "Pulse spreading and wandering in random media," *Radio Science*, Vol. 14, No. 5, 1979, pp. 925–931. doi:https://doi.org/10.1029/RS014i005p00925.

[16] Ostashev, V. E., Wilson, D. K., Collier, S. L., Cain, J. E., and Cheinet, S., "Cross-frequency coherence and pulse propagation in a turbulent atmosphere," *The Journal of the Acoustical Society of America*, Vol. 140, No. 1, 2016, pp. 678–691. doi:https://doi.org/10.1121/1.4959003.

[17] Sijtsma, P., "Acoustic array corrections for coherence loss due to the wind tunnel shear layer," Tech. Rep. NLR-TP-2008-112, NLR, February 2008.

[18] Rossignol, K.-S., and Delfs, J., "Analysis of the Noise Shielding Characteristics of a NACA0012 2D Wing," *22nd AIAA/CEAS Aeroacoustics Conference*, AIAA 2016-2795, Lyon, France, 30 May – 1 June 2016. doi:https://doi.org/10.2514/6.2016-2795.

[19] Rossignol, K.-S., Pott-Pollenske, M., Delfs, J., Silbermann, J., and Gomes, J., "Investigating Noise Shielding by Unconventional Aircraft Configurations," *23rd AIAA/CEAS Aeroacoustics Conference*, AIAA 2017-3195, Denver, Colorado, 5–9 June 2017. doi:https://doi.org/10.2514/6.2017-3195.

[20] Hutcheson, F. V., Bahr, C. J., Thomas, R. H., and Stead, D. J., "Experimental Noise Shielding Study for a NACA 0012 Airfoil," *24th AIAA/CEAS Aeroacoustics Conference*, AIAA 2018-2821, Atlanta, Georgia, 25–29 June 2018. doi:https://doi.org/10.2514/6.2018-2821.

[21] Qin, Q., and Attenborough, K., "Characteristics and application of laser-generated acoustic shock waves in air," *Applied Acoustics*, Vol. 65, No. 4, 2004, pp. 325–340. doi:https://doi.org/10.1016/j.apacoust.2003.11.003.

[22] Rossignol, K.-S., Delfs, J., and Boden, F., "On the Relevance of Convection Effects for a Laser-Generated Sound Source," *21st AIAA/CEAS Aeroacoustics Conference*, AIAA 2015-3146, Dallas, Texas, 22–26 June 2015. doi:https://doi.org/10.2514/6.2015-3146.

[23] Bahr, C., Zawodny, N. S., Yardibi, T., Liu, F., Wetzel, D., Bertolucci, B., and Cattafesta, L., "Shear layer time-delay correction using a non-intrusive acoustic point source," *International Journal of Aeroacoustics*, Vol. 10, No. 5–6, 2011, pp. 497–530. doi:https://doi.org/10.1260/1475-472X.10.5-6.497.

[24] Bahr, C. J., Zawodny, N. S., Bertolucci, B., Li, J., Sheplak, M., and Cattafesta, L. N., "A plasma-based non-intrusive point source for acoustic beamforming applications," *Journal of Sound and Vibration*, Vol. 344, 2015, pp. 59–80. doi: https://doi.org/10.1016/j.jsv.2015.01.023.

[25] Brown, K., Devenport, W., and Borgoltz, A., "Exploiting the Characteristics of Kevlar-Wall Wind Tunnels for Conventional Aerodynamic Measurements," *30th AIAA Aerodynamic Measurement Technology and Ground Testing Conference*, AIAA 2014-2110, Atlanta, Georgia, 16–20 June 2014. doi:https://doi.org/10.2514/6.2014-2110.

[26] Dougherty, R. P., "Advanced Time-domain Beamforming Techniques," *10th AIAA/CEAS Aeroacoustics Conference*, AIAA 2004-2955, Manchester, Great Britain, 10–12 May 2004. doi:https://doi.org/10.2514/6.2004-2955.

[27] Bahr, C. J., Hutcheson, F. V., and Stead, D. J., "Assessment of Unstead Propagation Characteristics and Corrections in Aeroacoustic Wind Tunnels Using an Acoustic Pulse," *24th AIAA/CEAS Aeroacoustics Conference*, AIAA 2018-3118, Atlanta, Georgia, 25–29 June 2018. doi:https://doi.org/10.2514/6.2018-3118.

[28] Wright, W. M., "Propagation in air of *N* waves produced by sparks," *The Journal of the Acoustical Society of America*, Vol. 73, No. 6, 1983, pp. 1948–1955. doi:https://doi.org/10.1121/1.389585.

[29] Yuldashev, P., Ollivier, S., Averiyanov, M., Sapozhnikov, O., Khokhlova, V., and Blanc-Benon, P., "Nonlinear propagation of spark-generated *N*-waves in air: Modeling and measurements using acoustical and optical methods," *The Journal of the Acoustical Society of America*, Vol. 128, No. 6, 2010, pp. 3321–3333. doi:https://doi.org/10.1121/1.3505106.

[30] Lipkens, B., and Blackstock, D. T., "Model experiment to study sonic boom propagation through turbulence. Part I: General results," *The Journal of the Acoustical Society of America*, Vol. 103, No. 1, 1998, pp. 148–158. doi:https://doi.org/10.1121/1.421114.

[31] Averiyanov, M., Ollivier, S., Khokhlova, V., and Blanc-Benon, P., "Random focusing of nonlinear acoustic *N*-waves in fully developed turbulence: Laboratory scale experiment," *The Journal of the Acoustical Society of America*, Vol. 130, No. 6, 2011, pp. 3595–3607. doi:https://doi.org/10.1121/1.3652869.

[32] Pascioni, K., Colangelo, A., and Cattafesta, L., "Acoustic Corrections for a Kevlar Wall Wind Tunnel Using a Pulsed-Laser Point Source," *24th International Congress on Sound and Vibration*, London, United Kingdom, 23–27 July 2017.

[33] *Method for Calculation of the Absorption of Sound by the Atmosphere*, ANSI S1.26-1995 (ASA 113-1995), Acoustical Society of America, 1995.

[34] Koop, L., Ehrenfried, K., and Kröber, S., "Investigation of the systematic phase mismatch in microphone-array analysis," *11th AIAA/CEAS Aeroacoustics Conference*, AIAA 2005-2962, Monterey, California, 23–25 May 2005. doi:https://doi.org/10.2514/6.2005-2962.

[35] *Condenser Microphones and Microphone Preamplifiers for acoustic measurements*, Brüel & Kjær, 1982.

[36] Schlinker, R. H., and Amiet, R. K., "Refraction and Scattering of Sound by a Shear Layer," Tech. Rep. NASA-CR-3371, United Technologies Research Center, 1981.